Size-Specific Reactions of Copper Cluster Ions with a Methanol Molecule

Masahiko Ichihashi,[†] Charlotte A. Corbett,[‡] Tetsu Hanmura,[§] James M. Lisy,[‡] and Tamotsu Kondow*[,†]

Cluster Research Laboratory, Toyota Technological Institute in East Tokyo Laboratory, Genesis Research Institute, Inc., 717-86 Futamata, Ichikawa, Chiba 272-0001, Japan, Department of Chemistry, University of Illinois at Urbana-Champaign, Urbana, Illinois 61801, and East Tokyo Laboratory, Genesis Research Institute, Inc., 717−86 Futamata, Ichikawa, Chiba 272-0001, Japan

Received: May 10, 2005

Chemisorption of a methanol molecule onto a size-selected copper cluster ion, Cu_n^+ ($n = 2-10$), and subsequent reactions were investigated in a gas-beam geometry at a collision energy less than 2 eV in an apparatus based on a tandem-type mass spectrometer. Mass spectra of the product ions show that the following two reactions occur after chemisorption: dominant formation of $Cu_{n-1}^+(H)(OH)$ (H(OH) formation) in the size range of 4−5 and that of Cu_nO^+ (demethanation) in the size range of 6−8 in addition to only chemisorption in the size range larger than 9. Absolute cross sections for the chemisorption, the H(OH) formation, and the demethanation processes were measured as functions of cluster size and collision energy. Optimized structures of bare copper cluster ions, reaction intermediates, and products were calculated by use of a hybrid method (B3LYP) consisting of the molecular orbital and the density functional methods. The origin of the size-dependent reactivity was explained as the structural change of cluster, two-dimensional to three-dimensional structures.

1. Introduction

A considerable number of studies on the size-dependent reactivity of metal clusters have been performed, since the cluster reactivity was found to depend critically on size. Actually, Whetten et al. have initiated size-specific adsorption of hydrogen molecules on neutral iron clusters; the adsorption rate becomes measurable above the size of 8 and changes dramatically with size.[1] Size-specific reactivity of charged metal clusters has been also discovered; for instance, three ethylene molecules were found to react into one benzene molecule only on Fe_4^+.[2] Recently we have measured the absolute cross sections for demethanation, chemisorption and carbide formation in collisions of nickel cluster ions, Ni_n^+, with a methanol molecule under single collision conditions and have discovered that demethanation proceeds preferentially on Ni_4^+, carbide formation on $Ni_{7,8}^+$, and chemisorption on Ni_6^+.[3]

Throughout these studies, it has been shown that the ionization energy, HOMO−LUMO gap, d-vacancies, and so on could be controlling parameters for determining the reactivity of metal clusters and their ions.[1,4−6] In particular, d-electrons play important roles in the reactions involving transition metal clusters, and both s- and d-electrons do so in those involving coinage metal clusters, because the valence electrons (d-electrons in the transition metal clusters and s- and d-electrons in the coinage metal clusters) participate in the reactions through stabilizing the electronic structures of the reaction intermediates, influencing electron correlation, electron localization and delocalization, electron−phonon coupling related to the reaction systems, and so on. The reactivity of a metal cluster changes with the cluster size because addition of even one atom to the cluster causes a change in these electronic characteristics of the cluster.

Coinage metal clusters have been investigated in a variety of ways, for instance, electronic shell structure, size distribution,[7,8] ionization potential,[9] photoelectron spectra,[10−13] bond dissociation energy,[14−16] ion mobility,[17] electrical dipole polarizability,[18] femtosecond dynamics,[19] and so on. These measurements have revealed the characteristics of the electronic and geometrical structures of the clusters. The fundamental feature of the electronic structures is well explained in terms of the spherical jellium model,[20] where the cluster is treated as a free electron gas of valence s-electrons and an averaged positive background of ionic cores. The geometrical structures have been illustrated by the ellipsoidal jellium model including corrections to the spherical jellium model.[20] For instance, Kappes and coworkers have explicated the geometrical structure of gold cluster cations, Au_n^+, by use of ion chromatography techniques and have found that Au_n^+ up to $n = 7$ have planar structures.[17] The density functional calculations have also elucidated the structures of coinage metal clusters.[21]

In addition to studies on the electronic structures of the coinage metal clusters, their reactivity has been investigated extensively because the coinage metals themselves exhibit catalytic activities of practical utility which differ from what open d-shell transition metals do, e.g., copper catalysts (Cu/ZnO, etc.) for methanol synthesis,[22] silver catalysts for ethylene oxidation,[23] nanosized gold catalysts,[24] etc. In the reaction of copper clusters with an oxygen molecule, it has been shown that the reactivity is correlated with filling of the electronic shells in the jellium model.[25] This finding itself manifests the involvement of delocalized valence electrons in the reaction. In the reaction of copper cluster ions, Cu_n^+ ($n = 1-14$) and Cu_n^- ($n = 4-13$), with carbon monoxide, they have no distinguishable size-

* To whom correspondence should be addressed.
[†] Toyota Technological Institute.
[‡] University of Illinois at Urbana-Champaign.
[§] Genesis Research Institute, Inc.

10.1021/jp0581577 CCC: $30.25
Published on Web 08/17/2005

dependent reactivity,[26,27] whereas neutral copper clusters, Cu_n, have a size-dependent reactivity with a prominently high reaction rate at $n = 16$ in the size range of $n = 15-20$.[28] This high reactivity is interpreted by an efficient symmetric matching between the HOMO and the LUMO of the copper cluster and the $2\pi^*$ and 5σ orbitals of a carbon monoxide. In recent computational studies, dissociative chemisorptions on copper clusters have been analyzed by using the density functional theory.[29,30]

In this article, we investigated the reaction of a copper cluster ion, Cu_n^+, with a methanol molecule through the measurement of the reaction cross sections as functions of the cluster size, in the size range of $n = 2-10$, and collision energy. We selected this reaction because of the practical importance of copper catalysts in methanol synthesis; the synthetic reaction proceeds on a cation site and the local density of the d-electron could contribute significantly.[31,32] In addition, Sharpe et al. have observed adsorption of a methanol molecule onto copper cluster cations, Cu_n^+ ($n = 1-3$ and 5), and have measured rate constants under multiple collision conditions.[33]

2. Experimental Section

A detailed description of the apparatus employed in this experiment has been reported elsewhere,[3] so that a brief description related to the present experiment is described here. The experimental apparatus is partitioned to regions of cluster ion production, cluster-size selection, reaction, and product analysis. Copper cluster ions were produced by an ion sputtering technique. Xenon ion beams from a plasma discharge ion gun (CORDIS Ar25/35c, Rokion Ionenstahl-Technologie) were accelerated up to 15 keV for bombardment of four copper plates (Nilaco, purity of 99.98%). Sputtered ions were extracted by a series of ion lenses and were admitted into an octopole ion beam guide (OPIG) located inside a cooling cell filled with helium gas ($\geq 10^{-1}$ Pa). The sputtered ions were cooled and decelerated in the OPIG in collision with helium atoms and mass-selected in a quadrupole mass filter (Extrel, 162−8) after passing through another OPIG. Size-selected cluster ions after passing through the mass filter were admitted into an OPIG surrounded by a reaction cell filled with methanol vapor ($10^{-3}-10^{-2}$ Pa), in which size-selected copper cluster ions react with methanol molecules under single collision conditions. Intact and product ions were mass-analyzed by another quadrupole mass filter and detected by a secondary electron multiplier with an ion-conversion dynode in its front so as to increase the detection efficiency. Signals from the detector were processed in a pulse counting manner.

The collision energy was controlled by changing the translational energy of Cu_n^+ in the reaction region, by varying a dc bias to the OPIG in the reaction cell with respect to the ground. At low collision energies, the velocity of a copper cluster ion is comparable to that of a methanol molecule, and hence the collision energy of the copper cluster ion with the methanol molecule was determined as follows: The distribution of the longitudinal energy distribution parallel to the beam axis of the copper cluster ions was measured by applying an electrostatic retarding potential at the OPIG surrounded by the reaction cell (electrostatic retarding method) and was converted to the distribution of the velocities of the ions parallel to the beam axis, where the energy distribution was assumed to be given by a Gaussian function. The distribution of the parallel velocities thus obtained is regarded as the true velocity distribution because the perpendicular velocities are much smaller than the parallel velocities. The velocity distribution of the methanol molecules in the reaction cell follows the Maxwell−Boltzmann distribution with a temperature of 300 K. The relative velocity distribution between a copper cluster ion and a methanol molecule was determined from the above velocity distributions by use of a Monte Carlo simulation technique and was employed for determining the collision energy and its uncertainty.

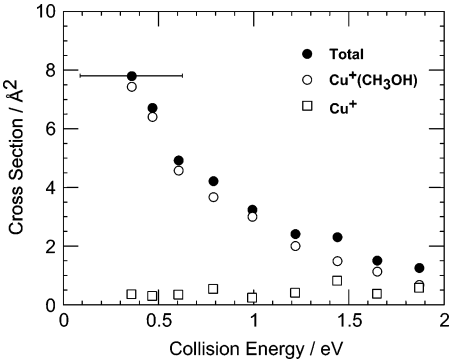

Figure 1. Total cross section and cross sections for formation of $Cu^+(CH_3OH)$ and Cu^+ in the collision of Cu_2^+ with a methanol molecule as a function of the collision energy. The uncertainty in the collision energy is shown as a horizontal bar.

3. Results

3.1. Reaction Cross Sections. Mass spectra of intact cluster ions, Cu_n^+, and product ions were measured up to $n = 10$ in the collision energy range of 0.2−2 eV. In the reaction of Cu_2^+ with CH_3OH, $Cu^+(CH_3OH)$ and Cu^+ were observed as product ions. Formation of these product ions indicates that the following reactions take place:

$$Cu_2^+ + CH_3OH \rightarrow Cu^+(CH_3OH) + Cu \quad (1)$$

$$Cu_2^+ + CH_3OH \rightarrow Cu^+ + Cu(CH_3OH) \quad (2)$$

Let us define the branching fraction for a given product ion, p_i, as

$$f_{pi} = I_{pi}/\Sigma_j I_{pj} \quad (3)$$

where I_{pi} and $\Sigma_j I_{pj}$ represent the intensity of a product ion, p_i, and the sum of the intensities of all the product ions observed, respectively. A total absolute reaction cross section, σ_r, was obtained as

$$\sigma_r = [k_B T/(Pl)] \log((I_r + \Sigma I_{pi})/I_r) \quad (4)$$

where I_r represents the intensity of an intact parent ion, P and T are the pressure and the temperature of methanol vapor, respectively, l (=120 mm) is the effective path length of the interaction region between the copper cluster ion beam and the methanol vapor, and k_B is Boltzmann's constant. A partial absolute reaction cross section, σ_{pi}, for the formation of a product ion is given by

$$\sigma_{pi} = f_{pi}\sigma_r \quad (5)$$

Figure 1 shows the total and the partial reaction cross sections for the products, $Cu^+(CH_3OH)$ and Cu^+, as a function of the collision energy. The reaction cross section for the formation of $Cu^+(CH_3OH)$ decreases with the increase of the collision energy, whereas that for the formation of Cu^+ seems to increase slightly with the collision energy. Both the reactions proceed via formation of a reaction intermediate, $Cu_2^+(CH_3OH)$, which

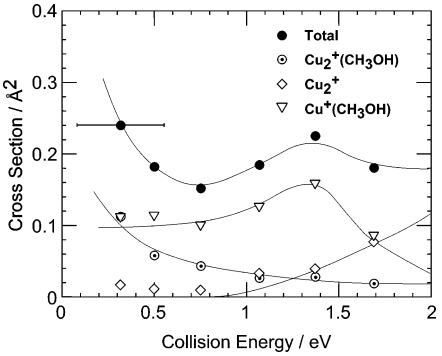

Figure 2. Total reaction cross section and cross sections for formation of $Cu_2^+(CH_3OH)$, Cu_2^+, and $Cu^+(CH_3OH)$ in the collision of Cu_3^+ with a methanol molecule as a function of the collision energy. The uncertainty in the collision energy is shown as a horizontal bar. Solid lines are guides to the eye.

dissociates into either $Cu^+(CH_3OH) + Cu$ or $Cu^+ + Cu(CH_3OH)$; $Cu^+(CH_3OH)$ or Cu^+ is detected finally as the product ion. The product ion, $Cu^+(CH_3OH)$, is much more abundant than Cu^+ probably because $Cu(CH_3OH)$ has a smaller ionization potential than Cu has, and energetically the formation of $Cu^+(CH_3OH)$ is favorable at low collision energies. At the collision energy of 1.9 eV, the cross section for the formation of Cu^+ becomes comparable with that for the formation of $Cu^+(CH_3OH)$. It is likely that collision-induced dissociation of Cu_2^+ begins to contribute to the formation of Cu^+ above the bond dissociation energy of 1.64−2.08 eV.[14,34,35]

Sharpe et al. have investigated the reaction of Cu_2^+ with CH_3OH by use of a Fourier transform ion cycrotron resonance mass spectrometer under multiple collision conditions[33] and have found that the formation of $Cu^+(CH_3OH)$ is the unique pathway. They have suggested that the bond dissociation energy between Cu^+ and CH_3OH is larger than that between Cu^+ and Cu. In the present experiment, the cross section for the reaction 1 decreases monotonically with the increase of the collision energy, and it is confirmed that this reaction proceeds without any significant activation energy barrier (see Figure 1).

In the reaction of Cu_3^+ with a methanol molecule, the following three reaction pathways are conceivable from the product ions:

$$Cu_3^+ + CH_3OH \rightarrow Cu_2^+(CH_3OH) + Cu \quad (6)$$

$$Cu_3^+ + CH_3OH \rightarrow Cu^+(CH_3OH) + Cu_2 \quad (7)$$

$$Cu_3^+ + CH_3OH \rightarrow Cu_2^+ + Cu(CH_3OH) \quad (8)$$

Figure 2 shows the cross sections of reactions 6−8 as a function of the collision energy. The total reaction cross section of Cu_3^+, which is the sum of the cross sections for reactions 6−8, is significantly smaller than that of Cu_2^+. At the collision energy of 0.3 eV, the cross section for reaction 8 (formation of Cu_2^+) is negligibly small. The cross section for reaction 6 (formation of $Cu_2^+(CH_3OH)$), which is comparable with that for reaction 7 (formation of $Cu^+(CH_3OH)$) at that collision energy, decreases with increasing collision energy; this tendency indicates that reaction 6 has no activation barrier. The smaller total reaction cross section of Cu_3^+ suggests that the reaction intermediate, $Cu_3^+(CH_3OH)$ dissociates rapidly back to Cu_3^+ and CH_3OH. This rapid dissociation is attributable to the stability of Cu_3^+ whose electron shell is closed in the jellium model.[20] At a collision energy of ≈1 eV, reaction 7 is the dominant reaction pathway. The cross section for reaction 8 increases with

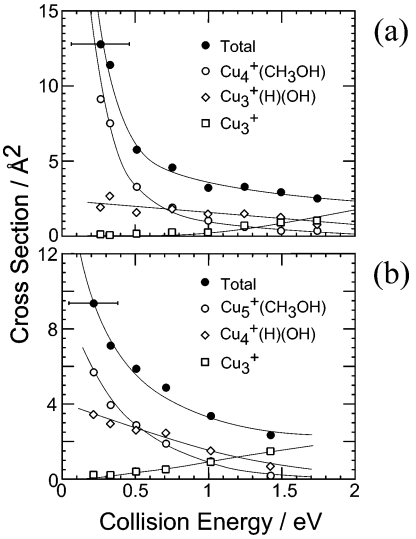

Figure 3. Cross sections for the collisions of Cu_4^+ (a) and Cu_5^+ (b) with a methanol molecule as a function of the collision energy. The uncertainty in the collision energy is shown as a horizontal bar. Solid lines are guides to the eye.

the collision energy. Sharpe et al. have also reported a low rate constant of reaction 6.[33]

For Cu_4^+ and Cu_5^+, the following three reaction pathways are conceivable on the basis of the product ions observed (n = 4 and 5):

$$Cu_n^+ + CH_3OH \rightarrow Cu_n^+(CH_3OH) \quad (9)$$

$$Cu_n^+ + CH_3OH \rightarrow Cu_{n-1}^+(H)(OH) + CuCH_2 \quad (10)$$

$$Cu_n^+ + CH_3OH \rightarrow Cu_3^+ + Cu_{n-3}(CH_3OH) \quad (11)$$

Figure 3 shows the reaction cross sections for Cu_4^+ and Cu_5^+ as a function of the collision energy. At a collision energy less than 0.5 eV, the formation of $Cu_n^+(CH_3OH)$ (chemisorption, reaction 9) is the dominant reaction pathway. With the increase of the collision energy, the cross section for the chemisorption decreases steeply, and instead the formation of $Cu_{n-1}^+(H)(OH)$ ((H(OH) formation, reaction 10) then becomes dominant at ≈1 eV. On the other hand, the cross section for the formation of Cu_3^+ (dissociation, reaction 11) increases gradually and tends to be dominant as the collision energy increases.

For Cu_n^+ (n = 6−8), the following two reaction pathways are considered to be opened:

$$Cu_n^+ + CH_3OH \rightarrow Cu_n^+(CH_3OH) \quad (12)$$

$$Cu_n^+ + CH_3OH \rightarrow Cu_nO^+ + CH_4 \quad (13)$$

Figure 4 shows the reaction cross sections of Cu_{6-8}^+ as a function of the collision energy. Both the cross sections for the formation of $Cu_n^+(CH_3OH)$ (chemisorption, reaction 12) and Cu_nO^+ (demethanation, reaction 13) decrease monotonically with the collision energy; and both of the reaction pathways have no significant activation barrier.

In the reaction of Cu_n^+ (n = 9 and 10) with CH_3OH, only $Cu_n^+(CH_3OH)$ was observed as the product ion. The cross section for the formation of $Cu_n^+(CH_3OH)$ decreases with the collision energy.

The cross sections for the chemisorptions, the H(OH) formation, and the demethanation are shown as a function of the cluster

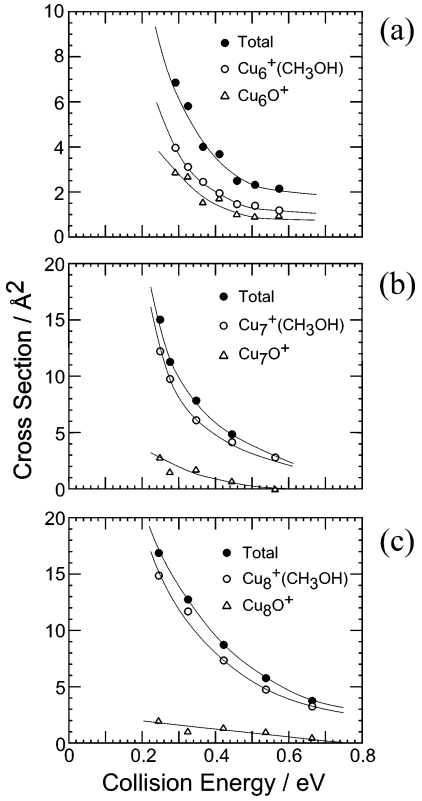

Figure 4. Cross sections for the collision of Cu_6^+ (a), Cu_7^+ (b), and Cu_8^+ (c) with a methanol molecule as a function of the collision energy. Solid lines are guides to the eye.

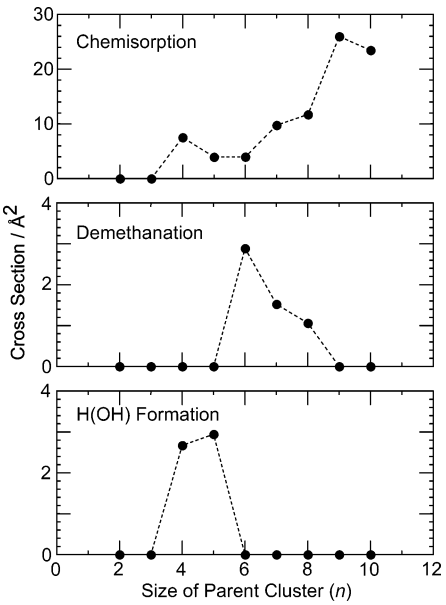

Figure 5. Cross sections for the H(OH) formation, the demethanation and the chemisorption as a function of the cluster size. The collision energy is 0.3 eV in the center-of-mass frame.

size at the collision energy of 0.3 eV as shown in Figure 5. The cross section for the chemisorption has a tendency to increase with the cluster size. The H(OH) formation proceeds only on Cu_n^+ ($n = 4$ and 5), and the cross section for the demethanation has a peak at $n = 6$ and decreases with the cluster size.

3.2. Structures and Energies of Cu_n^+. Energetics related to the reaction were obtained computationally for interpreting the energy- and size-dependent reactivity. To this end, the geometrical structures of the stable copper cluster ions, Cu_n^+ ($n = 2-9$), reaction intermediates, and the product ions ($Cu_n^+(CH_3OH)$, etc.) were calculated by using a hybrid method based on Hartree−Fock exchange and DFT exchange-correlation (Becke's three parameter hybrid method using the Lee−Yang−Parr correlation function, B3LYP) with the 6-311G basis sets. The calculation was performed by employing the Gaussian 98 suite of programs.[36]

Figure 6 shows the geometrical structures of copper cluster ions, Cu_n^+ ($n = 3-9$). In the geometry optimization, several two-dimensional and three-dimensional structures were chosen as initial structures. It was found that the structures are two-dimensional for $n \leq 7$ and three-dimensional for $n \geq 8$, though it has been reported that the structure change occurs between $n = 4$ and 5.[21,37,38]

In the present calculation, Cu_2^+ in the electronic ground state was found to have the bond length of 2.36 Å, which agrees well with the reported values, 2.36 Å[37] and 2.35 Å,[38] and reasonably well with that (2.39−2.42 Å) calculated by Gutsev and Bauschlicher.[35] The present calculation revealed that the optimized structure of Cu_3^+ has an equilateral triangle structure with the bond length of 2.32 Å, which has a very good agreement with the reported result (equilateral triangle, 2.39 Å,[21] 2.38 Å,[37] and 2.30 Å [38]). Similarly, our rhombic structure of Cu_4^+ with the bond length of 2.34 Å, is compared with reported rhombic structures with different bond lengths of 2.38 Å,[21] 2.43 Å,[37] and 2.35 Å[38] in the ground state.

On the other hand, the lowest-energy structures of ours are different from the reported structures in the size range of $n \geq 5$. Our calculation showed that the most stable Cu_5^+ has a butterfly-like structure, whereas a trigonal bipyramid structure has an energy higher by 0.69 eV than the butterfly structure has. On the other hand, the reported results revealed that a trigonal bipyramid is the most stable structure, whereas a butterfly-like structure has an energy higher by 0.45 eV than the trigonal bipyramid has.[37] In refs 21 and 38, the second lowest-energy isomer has a planar trapezoidal structure. In the present calculation of Cu_6^+ and Cu_7^+, they are found to have planar structures (crescent and hexagonal structures) that have lower energies than the other calculated structures, whereas in the most stable Cu_8^+ and Cu_9^+ two-atom capped and three atom-capped triangle structures are more stable than planar structures. In the refs 21 and 38, the lowest-energy structures of Cu_n^+ with $n = 6-9$ are a one-atom capped trigonal bipyramid, a pentagonal bipyramid, a two-atom capped octahedron, and a two-atom capped pentagonal bipyramid, respectively.

3.3. Energetics of $Cu_n^+ + CH_3OH$. In the reaction of Cu_2^+ with CH_3OH, reaction 1 is exothermic by 0.34 eV, and reaction 2 is endothermic by 1.21 eV on the basis of the present calculation. As shown in Figure 1, the measured cross section for reaction 1 is relatively large and decreases with the collision energy. On the other hand, reaction 2 looks endothermic (see Figure 1) because of the gradual increase of the cross section with the collision energy, although there is no clear indication of any threshold behavior in the collision-energy dependence of the cross section for reaction 2. The ambiguity of the threshold energy in the cross-section vs collision-energy plots of reaction 2 comes from the internal and the translational energy spread of Cu_2^+.

In the reaction of Cu_3^+ with CH_3OH, the present calculation shows that reaction 6 is endothermic by 0.79 eV but is still endothermic by 0.23 eV even if CH_3OH is bonded dissociatively to Cu_2^+ as $Cu_2^+(CH_3)(OH)$. Experimentally, $Cu_2^+(CH_3OH)$ is a product ion with a sizable intensity at a collision energy larger than 0.3 eV. It is likely that the CH_3OH bonded to Cu_2^+

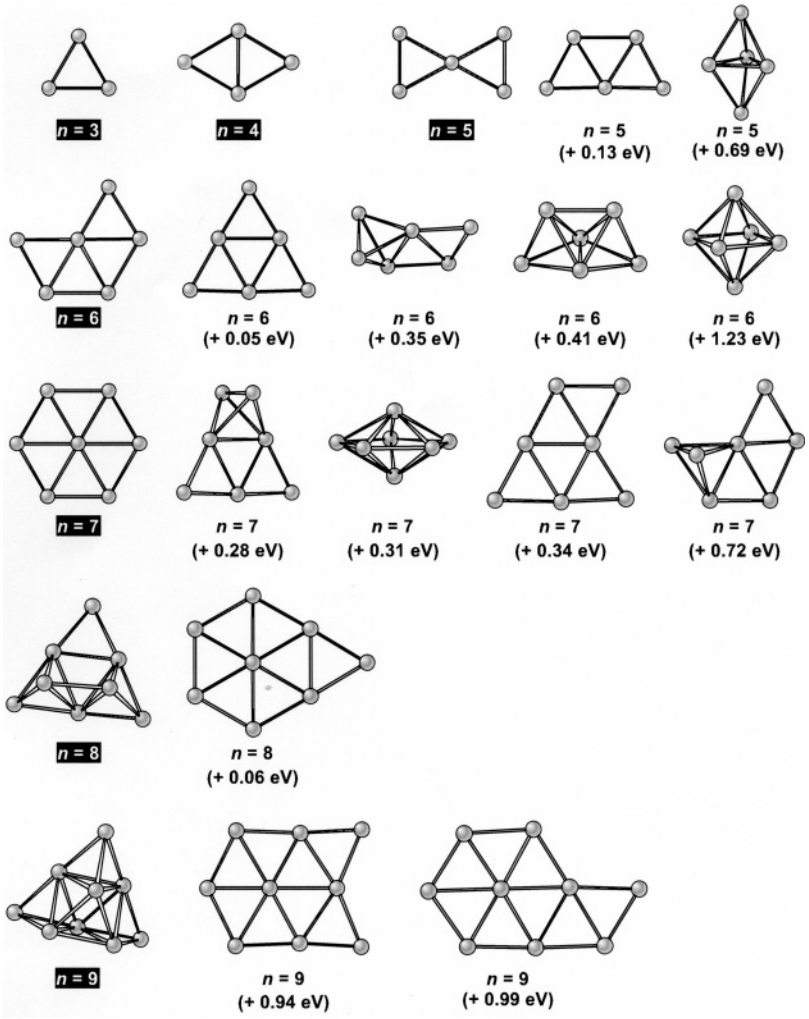

Figure 6. Optimized geometrical structures of Cu_n^+ ($n = 3-9$). Cluster sizes are indicated below the structures, where the outline characters show the lowest-energy structures. The values in the parentheses indicate the energies with respect to that of the lowest-energy structure.

dissociates to CH_3 and OH. On the other hand, reactions 7 and 8 proceed endothermically regardless of the structure of CH_3OH in $Cu^+(CH_3OH)$ and $Cu(CH_3OH)$.

As shown in Figure 2, reaction 6 has no activation energy barrier at a collision energy larger than 0.3 eV, because the cross section for reaction 6 decreases monotonically with the collision energy, whereas reactions 7 and 8 suggest the presence of an energy barrier because both the cross sections increase with increasing collision energy. The present calculation supports the presence of an energy barrier in these two reactions.

3.4. Transition States and Activation Energy Barriers. In the reactions of $Cu_{4,5}^+$ with CH_3OH, chemisorption (reaction 9), H(OH) formation (reaction 10), and dissociation (reaction 11) are found to proceed. Figure 7 shows a calculated potential energy curve for the $Cu_4^+ + CH_3OH$ reaction system in relation to the H(OH) formation through the chemisorption. As shown in Figure 7, the H(OH) formation proceeds exothermically. The present calculation gives reaction intermediates, $Cu_4^+(CH_3OH)$ (denoted as **A** in Figure 7), $Cu_4^+(OH)(CH_3)$ (denoted as **D** in Figure 7), $Cu_4^+(OCH_3)(H)$ (not shown in Figure 7), $Cu_4^+(H)(OH)(CH_2)$ (denoted as **F** in Figure 7), and $Cu_3^+(H)(OH)(CH_2)Cu$ (denoted as **G** in Figure 7), which are connected to the product channel, $Cu_3^+(H)(OH) + CuCH_2$. The reaction is shown to proceed by the calculation as follows: At first, a methanol molecule is chemisorbed onto an on-top site of Cu_4^+ at which the methanol molecule attaches most favorably to a copper atom having the highest positive net charge with the largest chemisorption energy (**A**). The dominant pathway is such that the chemisorbed methanol molecule dissociates into the hydroxy intermediate (**D**), which changes further into (**F**) and (**H**) before the products $Cu_3^+(H)(OH) + CuCH_2$. The hydroxy intermediate (**D**) is more likely as the reaction intermediate than the methoxy intermediate, $Cu_4^+(OCH_3)(H)$, because the former is more stable than the latter.

Structures and energies of several transition states on this potential energy curve were obtained by the present calculation, and the corresponding activation energy barriers were derived. To search the structure of a transition state located between (**A**) and (**C**), the bond length of C−O was fixed in the geometry optimization procedure. Optimized structures with different C−O bond lengths were obtained, and among them the structure with the maximum energy was determined as the energy of the transition state. The structures and the energies of the transition states thus obtained are shown in Figure 7. The energies are referenced with respect to the energy of the reactant system, $Cu_4^+ + CH_3OH$. The transition structures between (**C**) and (**D**), between (**D**) and (**F**), and between (**F**) and (**H**) were obtained similarly. The energies of these transition structures were found to be lower than that of the reactant. The exothermicity of the reaction system including all of the intermediate and the transition states is consistent with the collision-energy dependence of the total reaction cross section; the cross section for the overall reaction decreases sharply with the increase of the collision energy as shown in Figure 3. In contrast, the cross

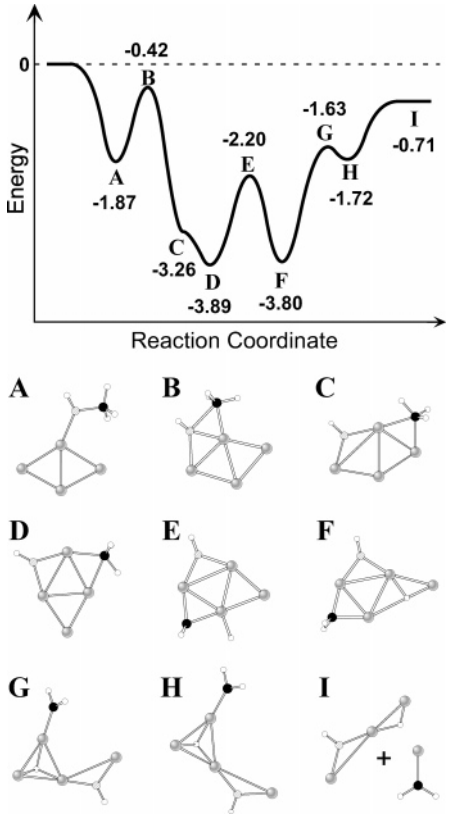

Figure 7. Potential energy curve of the reaction, $Cu_4^+ + CH_3OH \rightarrow Cu_3^+(H)(OH) + CuCH_2$. In the potential energy curve, the numbers written under **A** through **I** show the energies in the unit of eV of stable reaction intermediates, transition-state species and the final products indicated by **A** through **I**. Geometrical structures of **A** through **I** are illustrated, where hydrogen, oxygen, carbon, and copper atoms are shown as open, hatched, solid, and gray circles, respectively. The energies are referenced with respect to that of the initial state, $Cu_4^+ + CH_3OH$.

section for the H(OH) formation (reaction 10) decreases gradually with the collision energy and exceeds the cross section for reaction 9 at the collision energy of 1.75 eV. The dissociation (reaction 11) proceeds endothermically by 0.53 and 0.62 eV for $n = 4$ and 5, respectively. In both Cu_4^+ and Cu_5^+, the cross section for reaction 11 increases with the collision energy.

4. Discussion

4.1. Reaction of Cu_4^+ with CH_3OH. As described in the previous section, the reaction of Cu_4^+ with CH_3OH proceeds on the one-dimensional potential energy curve given in Figure 7. Initially, an incoming methanol molecule is captured in the electrostatic potential of Cu_4^+ as a weakly bound complex, $Cu_4^+\cdots(CH_3OH)$. The complex undergoes further reactions as

$$Cu_4^+ + CH_3OH \xleftarrow{k_0} Cu_4^+\cdots(CH_3OH) \quad (14)$$

$$Cu_4^+\cdots(CH_3OH) \xrightarrow{k_1} Cu_4^+(CH_3OH) \quad (15)$$

$$Cu_4^+\cdots(CH_3OH) \xleftarrow{k_2} Cu_4^+(CH_3OH) \quad (16)$$

$$Cu_4^+(CH_3OH) \xrightarrow{k_3} Cu_4^+(OH)(CH_3) \quad (17)$$

$$Cu_4^+(CH_3OH) \xleftarrow{k_4} Cu_4^+(OH)(CH_3) \quad (18)$$

$$Cu_4^+(OH)(CH_3) \xrightarrow{k_5} Cu_4^+(H)(OH)(CH_2) \quad (19)$$

$$Cu_4^+(OH)(CH_3) \xleftarrow{k_6} Cu_4^+(H)(OH)(CH_2) \quad (20)$$

$$Cu_4^+(H)(OH)(CH_2) \xrightarrow{k_7} Cu_3^+(H)(OH)(CH_2)Cu \quad (21)$$

$$Cu_4^+(H)(OH)(CH_2) \xleftarrow{k_8} Cu_3^+(H)(OH)(CH_2)Cu \quad (22)$$

$$Cu_3^+(H)(OH)(CH_2)Cu \xrightarrow{k_9} Cu_3^+(H)(OH) + CuCH_2 \quad (23)$$

Suppose that these reactions obey the rate equations as

$$d[Cu_4^+\cdots(CH_3OH)]/dt = -(k_0 + k_1)[Cu_4^+\cdots(CH_3OH)] + k_2[Cu_4^+(CH_3OH)] \quad (24)$$

$$d[Cu_4^+(CH_3OH)]/dt = k_1[Cu_4^+\cdots(CH_3OH)] - (k_2 + k_3)[Cu_4^+(CH_3OH)] + k_4[Cu_4^+(OH)(CH_3)] \quad (25)$$

$$d[Cu_4^+(OH)(CH_3)]/dt = k_3[Cu_4^+(CH_3OH)] - (k_4 + k_5)[Cu_4^+(OH)(CH_3)] + k_6[Cu_4^+(H)(OH)(CH_2)] \quad (26)$$

$$d[Cu_4^+(H)(OH)(CH_2)]/dt = k_5[Cu_4^+(OH)(CH_3)] - (k_6 + k_7)[Cu_4^+(H)(OH)(CH_2)] + k_8[Cu_3^+(H)(OH)(CH_2)Cu] \quad (27)$$

$$d[Cu_3^+(H)(OH)(CH_2)Cu]/dt = k_7[Cu_4^+(H)(OH)(CH_2)] - (k_8 + k_9)[Cu_3^+(H)(OH)(CH_2)Cu] \quad (28)$$

$$d[Cu_3^+(H)(OH)]/dt = k_9[Cu_4^+(H)(OH)(CH_2)] \quad (29)$$

where [X] shows the intensity of X. These equations were solved by using a recursion formula

$$[X](t = t_{i+1}) = [X](t = t_i) + (d[X]/dt)(t = t_i)\Delta t \quad (30)$$

The time step, Δt, was set to be 0.1 ps, and the intensity of each ion was calculated sequentially. In the RRK framework,[39,40] a rate constant, k_j, is given by

$$k_j = A_j \{(E_{init} + E_{col} + E_{B_j} - E_{A_j})/(E_{init} + E_{col} + E_{B_j})\}^{L-1} \quad (31)$$

where A_j is the prefactor obtained from the degeneracy and the vibrational frequency of an internal mode related to the reaction coordinate, E_{init}, E_{col}, E_{B_j}, and E_{A_j} are the internal energies of Cu_4^+ and CH_3OH before the collision, the collision energy, the binding energy of the jth species to Cu_4^+ and the activation energy barrier to get into Cu_4^+(jth species), respectively, and L is the total number of the vibrational modes of $Cu_4^+(CH_3OH)$. The reaction time is experimentally obtained to be $\approx$100 μs as the flight time of the ion of interest from the reaction cell to the entrance slit of the second quadrupole mass filter, where scattering and deceleration of the ions in collision with methanol molecules is ignored in the estimation of the flight time.

A partial reaction cross section was obtained by the equation

$$\sigma_{pi\_calc} = \sigma_L([X_i]/\Sigma_j[X_j]) \quad (32)$$

where σ_L represents the Langevin cross section for the capture of a CH_3OH molecule by Cu_4^+, and is given as π ($2\alpha/E_{col}$) with α of the polarizability of CH_3OH. Figure 8 shows the cross

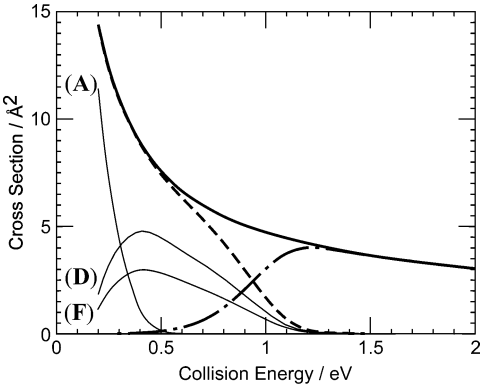

Figure 8. Reaction cross sections calculated by using the potential energy curve shown in Figure 7 in the framework of RRK theory. Thick solid, dashed, and alternate long and short dashed lines show the total cross section and those for chemisorption and H(OH) formation, where the chemisorption cross section is the sum of the cross sections for the formation of $Cu_4^+(CH_3OH)$ (**A**), $Cu_4^+(OH)(CH_3)$ (**D**), and $Cu_4^+(H)(OH)(CH_3)$ (**F**).

TABLE 1: Prefactors, A_j, Used in the RRK Calculation

A_0	A_1	A_2	A_3	A_4
3×10^{12}/s	2×10^{13}/s	2×10^{13}/s	2×10^{13}/s	9×10^{13}/s
A_5	A_6	A_7	A_8	A_9
4.5×10^{13}/s	4.5×10^{13}/s	9×10^{13}/s	4.5×10^{13}/s	1.5×10^{13}/s

sections thus obtained as a function of the collision energy. The prefactor, A_j, was approximated by the vibrational frequency related to the reaction pathway concerned (see Table 1). The reaction cross sections for the formation of (**A**), (**D**), and (**F**) in addition to that of $Cu_3^+(OH)(H) + CuCH_2$ are plotted as a function of the collision energy in Figure 8. Note that there is no experimental evidence one way or the other to support that the methanol molecule is dissociatively chemisorbed.

As shown in Figure 8, there are several features in the collision-energy dependence of the calculated cross sections as explained above. The total reaction cross section decreases with the increase of the collision energy. As the collision energy increases, the cross section for the formation of (**A**), which is the most abundant in the energy range less than 0.3 eV, decreases rapidly, whereas the cross sections for the formation of (**D**) and (**F**), which exceed the cross section for (**A**) in the energy range above 0.3 eV, increase rapidly and then decrease after passing the maximum at ≈0.4 eV. The cross section for the formation of $Cu_3^+(H)(OH)$, which become the most dominant above ≈1.0 eV, starts to increase at ≈0.5 eV. The calculation is compared with the experimental results (see Figure 3). As the collision energy increases, the calculated cross section for the formation of $Cu_3^+(H)(OH)$ starts to increase at ≈0.5 eV, whereas the experimental one decreases monotonically. The sum of the calculated cross sections for the formation of (**A**), (**D**), and (**F**) agrees well with the experimental cross section for the formation of $Cu_4^+(CH_3OH)$. Presumably, the excess energy of the reaction intermediates is not distributed equally to all of the vibrational modes but to a limited number of the vibrational modes involved in the formation of $Cu_3^+(H)(OH) + CuCH_2$.

4.2. Reaction of Cu_6^+ with CH_3OH. It was shown experimentally that the chemisorption and the demethanation take place but H(OH) formation does not on Cu_n^+ ($n = 6-8$) by a single collision with a methanol molecule, in the entire collision energy range studied. On the other hand, the optimized structures of reaction intermediates of the $Cu_6^+ + CH_3OH$ reaction system

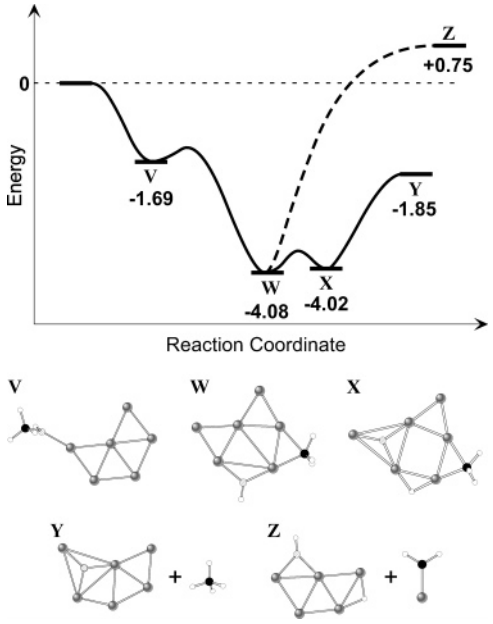

Figure 9. Schematic potential energy curve for the reaction, $Cu_6^+ + CH_3OH \rightarrow Cu_6O^+ + CH_4$, and $Cu_6^+ + CH_3OH \rightarrow Cu_5^+(H)(OH) + CuCH_2$. In the potential energy curve, the numbers written under **V** through **Z** show the energies (in the unit of eV) of the reaction intermediates (**V**, **W**, and **X**) and the final products (**Y** and **Z**). Geometrical structures of **V** through **Z** are illustrated, where hydrogen, oxygen, carbon, and copper atoms are shown as open, hatched, solid, and gray circles, respectively. The energies are referenced with respect to that of the initial state, $Cu_6^+ + CH_3OH$.

were obtained computationally, and a schematic potential energy curve by taking the energies of the reaction intermediates into consideration is illustrated in Figure 9. A methanol molecule bound to an on-top site of Cu_6^+ (denoted as **V** in Figure 9) can dissociate into $OCH_3 + H$ (methoxy intermediate, not shown in Figure 9) or into $OH + CH_3$ (hydroxy intermediate, denoted as **W** in Figure 9) similarly to Cu_4^+; however, the latter, $Cu_6^+(OH)(CH_3)$ (**W**), is more stable than the former, $Cu_6^+(OCH_3)(H)$. On this hydroxy intermediate (**W**), the hydroxy group dissociates further into H and O (**X**), and then H reacts with CH_3 into CH_4 on Cu_6^+; CH_4 is released from Cu_6O^+ (**Y**). The chemisorption (reaction 12) and the demethanation occur but the H(OH) formation does not, because the chemisorption and the demethanation are exothermic, but H(OH) formation is endothermic by 0.75 eV.

4.3. Reaction of Cu_9^+ with CH_3OH. We calculated stable structures of $Cu_9^+(CH_3OH)$ and Cu_9O^+ which include several isomers but not all, because our structure survey was not complete. On the basis of the calculation, we conclude that the following reaction pathways are exothermic:

$$Cu_9^+ + CH_3OH = Cu_9^+(CH_3OH) + 1.54\ \text{eV} \quad (33)$$

$$Cu_9^+ + CH_3OH = Cu_9O^+ + CH_4 + 1.74\ \text{eV} \quad (34)$$

As shown above, the formation of Cu_9O^+ is exothermic, but this species is not observed experimentally. We showed experimentally that $Cu_9^+(CH_3OH)$ formation by the reaction of Cu_9^+ with a CH_3OH molecule has a sizable reaction cross section (see Figure 5). It is likely that $Cu_9^+(OH)(CH_3)$, etc. is more stable than $Cu_9^+(CH_3OH)$ as are the cases of Cu_4^+ and Cu_6^+, although the structures of $Cu_9^+(OH)(CH_3)$, etc., in which a methanol molecule is dissociatively chemisorbed on Cu_9^+, have not been calculated yet. Similar discussion is applicable to the reaction involving Cu_{10}^+ with CH_3OH.

4.4. Size-Dependent Reactivity. *Chemisorption, $Cu_n^+ + CH_3OH \rightarrow Cu_n^+(CH_3OH)$.* In the entire cluster size range studied, we observed the product ion, $Cu_n^+(CH_3OH)$, in the reaction of Cu_n^+ with CH_3OH; in the cluster size ≤ 3, one Cu atom (formation of $Cu_{n-1}^+(CH_3OH)$) is found be liberated for releasing the energy of the reaction because of a limited number of freedom in such a small cluster ion. Computationally, it is shown that $Cu_n^+(OH)(CH_3)$ is energetically more stable than $Cu_n^+(CH_3OH)$, and both of the species are present as the reaction intermediates. Experimentally, it is impossible to distinguish the two species.

Let us examine the collision-energy dependence of the branching fraction of the two species, $Cu_n^+(OH)(CH_3)$ and $Cu_n^+(CH_3OH)$, obtained by the calculation. In a low collision energy as low as $\approx$0.3 eV, the dominant reaction intermediate is $Cu_n^+(CH_3OH)$ and is switched gradually to $Cu_n^+(OH)(CH_3)$ as the collision energy increases. The structure of Cu_n^+ itself is not deformed by the chemisorption whether the chemisorption is dissociative or nondissociative.

As shown in Figure 5, the cross section for the chemisorption (dissociative + nondissociative) has an increasing tendency with the cluster size. The cross section for an incoming CH_3OH molecule being captured in the electrostatic potential of Cu_n^+ (Langevin cross section) turns out to be 56 Å^2 at the collision energy of 0.3 eV. On the other hand, the experimental cross section for the chemisorption is as small as $\approx$7 Å^2 at the collision energy of 0.3 eV and has a tendency to increase with the cluster size. This result suggests that the once captured CH_3OH should have a high probability of being desorbed from Cu_n^+. The lifetimes of the reaction intermediates, $Cu_n^+(CH_3OH)$ and $Cu_n^+(CH_3)(OH)$, tend to increase with increasing the cluster size.

H(OH) Formation, $Cu_n^+ + CH_3OH \rightarrow Cu_{n-1}^+(H)(OH) + CuCH_2$. It is experimentally shown that this reaction takes place only on $Cu_{4,5}^+$ (see Figure 5), because the H(OH) formation is exothermic only for $n = 4$ and 5 based on the present calculations. These energetics are explained on the basis of structural considerations. The calculation shows that a considerable structural change occurs when Cu_4^+ reacts with a CH_3OH molecule into $Cu_3^+(H)(OH) + CuCH_2$. The cluster ion, Cu_4^+, has a rhombic structure, but Cu_3^+ in $Cu_3^+(H)(OH)$ has a linear structure, probably because H and OH prefer copper atoms with reduced Cu−Cu interactions. As the cluster size increases, the H(OH) formation becomes less likely probably because it becomes more difficult to take on the preferred linear form of the H(OH) reaction intermediate. In the reaction involving a large cluster ion, Cu_n^+, Cu_{n-1}^+ in the H(OH) reaction intermediate would have a two-dimensional structure resulting in a higher energy barrier to H(OH) formation.

Demethanation, $Cu_n^+ + CH_3OH \rightarrow Cu_nO^+ + CH_4$. The demethanation proceeds only on Cu_n^+ ($n = 6-8$); among the cluster ions, Cu_6^+ has the largest cross section for demethanation, which decreases with cluster size. The calculations show, as mentioned in the sections 4.2 and 4.3, that demethanation proceeds exothermically both on Cu_6^+ and Cu_9^+, whereas the experiment shows that demethanation proceeds on Cu_6^+ but not on Cu_9^+. This phenomenon has two possible explanations; (1) a lifetime of the reaction intermediates in the reaction involving Cu_9^+ is too long to be observed and (2) an energy barrier between the reaction intermediate and the final product is too high for the reaction to take place. As for the former, the chemisorption energy does not depend greatly on the cluster size, and the available energy of the reaction intermediates does not change with the cluster size, whereas their degrees of freedom increase with cluster size. Then, the reaction rate decreases with the cluster size. As for the latter, it is likely that the energy barrier increases with the cluster size, and the demethanation does not proceed efficiently. For instance, in Cu_6O^+, the oxygen atom sits at the center of a triangle unit of Cu_6O^+, whereas in Cu_9O^+, the oxygen atom sits at the center of a tetrahedral unit. In both cases, the Cu−Cu bond of the unit should elongate considerably when an oxygen atom bonds to it. The energy of the elongation depends on the cluster structure which changes with the cluster size. The energy of elongation increases with the cluster size as suggested by the calculation.

5. Conclusion

Copper cluster ions, Cu_n^+ ($n = 2-10$), were shown to have size specific reactivity with a methanol molecule; H(OH) formation proceeds at $n = 4$ and 5, and demethanation proceeds at $n = 6-8$. To elucidate the reaction mechanisms, potential energy curves were obtained by use of a quantum mechanical calculation based on a hybrid method, and possible reaction pathways were shown. In the reaction of Cu_4^+ with a CH_3OH molecule, the absolute reaction cross sections obtained experimentally were successfully reproduced by using the potential energy curve in the framework of RRK theory and Langevin cross section. Similarly, the reaction of Cu_6^+ with a CH_3OH molecule was also explained qualitatively by using the energies of the reaction intermediates and the final products. The size-dependent reactivity was interpreted within the concept of structural flexibility. Time-dependent measurements on this reaction facilitate elucidating the origin of the size-dependent reactivity of the cluster ions.

Acknowledgment. Most of the calculations were performed by NEC SX-7, TX-7, and SGI 2800 of the Research Center for Computational Science, Okazaki Research Facilities, National Institutes of Natural Sciences. The participation of C.A.C and J.M.L. was made possible by support of the U.S. National Science Foundation [NSF] (Grant INT-9726311). Subsequent participation by J.M.L. was made possible by the U.S. NSF (Grant CHE 0415859).

References and Notes

(1) Whetten, R. L.; Cox, D. M.; Trevor, D. J.; Kaldor, A. *Phys. Rev. Lett*. **1985**, *54*, 1494.
(2) Schnabel, P.; Irion, M. P.; Weil, K. G. *J. Phys. Chem.* **1991**, *95*, 9688.
(3) Ichihashi, M.; Hanmura, T.; Yadav, R. T.; Kondow, T. *J. Phys. Chem. A* **2000**, *104*, 11885.
(4) Conceição, J.; Laaksonen, R. T.; Wang, L.-S.; Guo, T.; Nordlander, P.; Smalley, R. E. *Phys. Rev. B* **1995**, *51*, 4668.
(5) Kietzmann, H.; Morenzin, J.; Bechthold, P. S.; Ganteför, G.; Eberhardt, W. *J. Chem. Phys.* **1998**, *109*, 2275.
(6) Yadav, R. T.; Ichihashi, M.; Kondow, T. *J. Phys. Chem. A* **2004**, *108*, 7188.
(7) Powers, D. E.; Hansen, S. G.; Geusic, M. E.; Michalopoulos, D. L.; Smalley, R. E. *J. Chem. Phys.* **1983**, *78*, 2866.
(8) Katakuse, I.; Ichihara, T.; Fujita, Y.; Matsuo, T.; Sakurai, T.; Matsuda, H. *Int. J. Mass Spectrom. Ion Processes* **1985**, *67*, 611.
(9) Knickelbein, M. B. *Chem. Phys. Lett*. **1992**, *192*, 129.
(10) Ho, J.; Ervin, K. M.; Lineberger, W. C. *J. Chem. Phys*. **1990**, *93*, 6987.
(11) Taylor, K. J.; Pettiette-Hall, C. L.; Cheshnovsky, O.; Smalley, R. E. *J. Chem. Phys.* **1992**, *96*, 3319.
(12) Häkkinen, H.; Yoon, B.; Landman, U.; Li, X.; Zhai, H.-J.; Wang, L.-S. *J. Phys. Chem. A* **2003**, *107*, 6168.
(13) von Gynz-Rekowski, F.; Bertram, N.; Ganteför, G.; Kim, Y. D. *J. Phys. Chem. B* **2004**, *108*, 18916.
(14) Ingólfsson, O.; Busolt, U.; Sugawara, K. *J. Chem. Phys.* **2000**, *112*, 4613.
(15) Krückeberg, S.; Schweikhard, L.; Ziegler, J.; Dietrich, G.; Lützenkirchen, K.; Walther, C. *J. Chem. Phys*. **2001**, *114*, 2955.

(16) Spasov, V. A.; Lee, T.-H.; Ervin, K. M. *J. Chem. Phys.* **2000**, *112*, 1713.

(17) Gilb, S.; Weis, P.; Furche, F.; Ahlrichs, R.; Kappes, M. M. *J. Chem. Phys*. **2002**, *116*, 4094.

(18) Knickelbein, M. B. *J. Chem. Phys.* **2004**, *120*, 10450.

(19) Bernhardt, T. M.; Hagen, J.; Socaciu, L. D.; Mitric, R.; Heidenreich, A.; Le Roux, J.; Popolan, D.; Vaida, M.; Wöste, L.; Bonačić-Koutecký, V.; Jortner, J. *ChemPhysChem* **2005**, *6*, 243.

(20) Brack, M. *Rev. Mod. Phys*. **1993**, *65*, 677.

(21) Fernández, E. M.; Soler, J. M.; Garzón, I. L.; Balbás, L. C. *Phys. Rev. B* **2004**, *70*, 165403 and references therein.

(22) Chinchen, C. G.; Denny, P. J.; Jennings, J. R.; Spencer, M. S.; Waugh, K. C. *Appl. Catal*. **1988**, *36*, 1.

(23) Backx, C.; de Groot, C. P. M.; Biloen, P.; Sachtler, W. M. H. *Surf. Sci*. **1983**, *128*, 81 and references therein.

(24) Haruta, M. *Catal. Today* **1997**, *36*, 153.

(25) Andersson, M.; Persson, J. L.; Rosén, A. *J. Phys. Chem*. **1996**, *100*, 12222.

(26) Leuchtner, R. E.; Harms, A. C.; Castleman, A. W., Jr. *J. Chem. Phys*. **1990**, *92*, 6527.

(27) Lee, T. H.; Ervin, K. M. *J. Phys. Chem*. **1994**, *98*, 10023.

(28) Holmgren, L.; Gronbeck, H.; Andersson, M.; Rosén, A. *Phys. Rev. B* **1996**, *53*, 16644.

(29) Yamin, L. J.; Gómez, M. F.; Arrúa, L. A. *J. Mol. Struct. (THEOCHEM)* **2004**, *684*, 159.

(30) Guvelioglu, G. H.; Ma, P.; He, X.; Forrey, R. C.; Cheng, H. *Phys. Rev. Lett.* **2005**, *94*, 026103.

(31) Herman, R. G.; Kleir, K.; Simmons, G. W.; Finn, B. P.; Bulko, J. B. *J. Catal*. **1979**, *56*, 407.

(32) Mehta, S.; Simmons, G. W.; Klier, K.; Herman, R. G. *J. Catal*. **1979**, *57*, 339.

(33) Sharpe, P.; Campbell, J. M.; Cassady, C. J. *Organometallics* **1994**, *13*, 3077.

(34) Rohlfing, E. A.; Valentini, J. J. *J. Chem. Phys.* **1986**, *84*, 6560.

(35) Gutsev, G. L.; Bauschlicher, C. W., Jr. *J. Phys. Chem. A* **2003**, *107*, 4755.

(36) Frisch, M. J.; Trucks, G. W.; Schlegel, H. B.; Scuseria, G. E.; Robb, M. A.; Cheeseman, J. R.; Zakrzewski, V. G.; Montgomery, J. A., Jr.; Stratmann, R. E.; Burant, J. C.; Dapprich, S.; Millam, J. M.; Daniels, A. D.; Kudin, K. N.; Strain, M. C.; Farkas, O.; Tomasi, J.; Barone, V.; Cossi, M.; Cammi, R.; Mennucci, B.; Pomelli, C.; Adamo, C.; Clifford, S.; Ochterski, J.; Petersson, G. A.; Ayala, P. Y.; Cui, Q.; Morokuma, K.; Malick, D. K.; Rabuck, A. D.; Raghavachari, K.; Foresman, J. B.; Cioslowski, J.; Ortiz, J. V.; Stefanov, B. B.; Liu, G.; Liashenko, A.; Piskorz, P.; Komaromi, I.; Gomperts, R.; Martin, R. L.; Fox, D. J.; Keith, T.; Al-Laham, M. A.; Peng, C. Y.; Nanayakkara, A.; Gonzalez, C.; Challacombe, M.; Gill, P. M. W.; Johnson, B. G.; Chen, W.; Wong, M. W.; Andres, J. L.; Head-Gordon, M.; Replogle, E. S.; Pople, J. A. *Gaussian 98*, revision A.11.3; Gaussian, Inc.: Pittsburgh, PA, 1998.

(37) Calaminici, P.; Köster, A. M.; Russo, N.; Salahub, D. R. *J. Chem. Phys*. **1996**, *105*, 9546.

(38) Jug, K.; Zimmermann, B.; Calaminici, P.; Köster, A. M. *J. Chem. Phys*. **2002**, *116*, 4497.

(39) Rice, O. K.; Ramsperger, H. C. *J. Am. Chem. Soc*. **1927**, *49* 1617.

(40) Kassel, L. S. *J. Phys. Chem*. **1928**, *32*, 225.